Int J Thermophys (2009) 30:934–948
DOI 10.1007/s10765-009-0587-1

Influence of Spacer Systems on Heat Transfer in Evacuated Glazing

K. Swimm · H. Weinläder · H.-P. Ebert

Received: 4 October 2007 / Accepted: 27 April 2009 / Published online: 19 May 2009

Abstract One attractive possibility to essentially improve the insulation properties of glazing is to evacuate the space between the glass panes. This eliminates heat transport due to convection between the glass panes and suppresses the thermal conductivity of the remaining low pressure filling gas atmosphere. The glass panes can be prevented from collapsing by using a matrix of spacers. These spacers, however, increase heat transfer between the glass panes. To quantify this effect, heat transfer through samples of evacuated glazing was experimentally determined. The samples were prepared with different kinds of spacer materials and spacer distances. The measurements were performed with a guarded hot-plate apparatus under steady-state conditions and at room temperature. The measuring chamber of the guarded hot plate was evacuated to $<10^{-2}$ Pa. An external pressure load of 0.1 MPa was applied on the samples to ensure realistic system conditions. Radiative heat transfer was significantly reduced by preparing the samples with a low-ε coating on one of the glass panes. In a first step, measurements without any spacers allowed quantification of the amount of radiative heat transfer. With these data, the measurements with spacers could be corrected to separate the effect of the spacers on thermal heat transfer. The influence of the thermal conductivity of the spacer material, as well as the distance between the spacers and the spacer geometry, was experimentally investigated and showed good agreement with simulation results. For mechanically stable matrices with cylindrical spacers, experimental thermal conductance values $\leq 0.44\,\mathrm{W \cdot m^{-2} \cdot K^{-1}}$ were found. This shows that U_g-values of about $0.5\,\mathrm{W \cdot m^{-2} \cdot K^{-1}}$ are achievable in evacuated glazing, if highly efficient low-emissivity coatings are used.

K. Swimm (✉) · H. Weinläder · H.-P. Ebert
Functional Materials for Energy Technology, Bavarian Center for Applied Energy Research,
Am Hubland, 97074 Würzburg, Germany
e-mail: swimm@zae.uni-wuerzburg.de

Keywords Hot-plate apparatus · Thermal conductance · Thermal contact resistance · Vacuum insulation glass

1 Introduction

The thermal insulation properties of façade elements are described by the thermal transmittance U, which is calculated from the thermal conductance Λ and the heat transfer coefficients α_i and α_e at the interior and exterior surfaces, respectively:

$$U = \left(\frac{1}{\alpha_i} + \frac{1}{\Lambda} + \frac{1}{\alpha_e} \right)^{-1} . \tag{1}$$

For most insulation materials, Λ can be determined by adding up the heat transfer contributions of solid and gaseous conduction, as well as radiation. Disregarding edge effects, the thermal transmittance in the center of a glazing is called the U_g-value.

In modern buildings with well insulated walls ($U < 0.3\,\mathrm{W \cdot m^{-2} \cdot K^{-1}}$), conventional double-glazed windows ($U_g \approx 1.1\,\mathrm{W \cdot m^{-2} \cdot K^{-1}}$) represent thermal weak spots in the façade. One possibility to improve the insulation properties of glazing is to evacuate the space between the glass panes. This reduces heat transfer due to gaseous conduction to a negligible level at gas pressures lower than 0.1 Pa [1,2]. To prevent the window from collapsing, a matrix of spacers has to be set between the glass sheets (Fig. 1). Heat conduction through the spacers, however, increases the overall heat transfer through the window. Therefore, the design of the spacers needs to be optimized regarding the thermal properties. In order to guarantee good insulating properties, a highly efficient low-emissivity coating is also essential, to reduce the radiative heat transfer between the two glass panes.

A research group at the University of Sydney performed measurements of local heat flow through samples of evacuated glazing with a small area (1.7 $\mathrm{cm^2}$) guarded hot plate apparatus [3]. The simple addition of the separate heat transfer mechanisms, which are heat conduction through the spacers and the edge seal, conduction by the

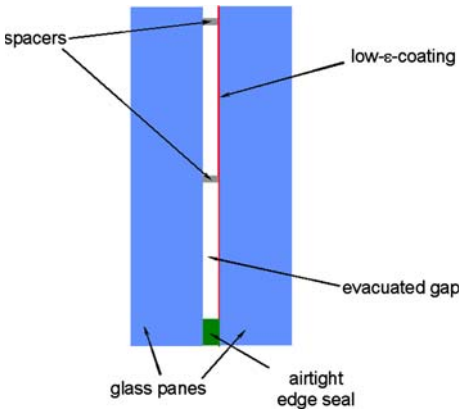

Fig. 1 Diagram of a vacuum insulation glass with two 4 mm thick float glass panes (system thickness < 9 mm)

residual gas and radiative heat transfer, is in good agreement with overall heat transmission coefficients measured in a guarded hot box [4]. It was also shown that the thermal resistance of spacers with very little height and a much higher thermal conductivity than glass can be neglected and the heat conduction through a spacer in vacuum insulation glass (VIG) can be described only by the spreading heat flow in the glass sheets:

$$\Lambda'_{\mathrm{spac}} \approx 2 r_{\mathrm{spac}} \lambda_{\mathrm{glass}}, \tag{2}$$

where Λ'_{spac} is the thermal conductance of a single spacer, r_{spac} is the spacer radius, and λ_{glass} is the thermal conductivity of the glass sheets [5]. However, this approximation is not valid for the spacers that were investigated within the scope of this paper, because their height (1 mm) is generally comparable to their diameter. Therefore, a theoretical study of the problem was carried out by finite-difference modeling (HEAT3). In addition, the spacers investigated show substantial surface roughness at the end faces, which could cause a contact resistance between the glass panes and spacers. The experimental investigation of the thermal properties of different spacer systems took place in an evacuable guarded hot-plate apparatus [6].

Besides, the mechanical stability of the window must not be neglected. Collins and Fischer-Cripps [7] constituted several design criteria for vacuum insulation glass, which regard both mechanical and thermal aspects. One goal of this work was to compare the thermal conductances of different spacer arrays, which were arrays of cylinders or spheres with distances from 2 cm to 4 cm. Some of them are mechanically inappropriate; this will be pointed out later. The main goal was to find out if the desired U_{g}-value of $0.5\,\mathrm{W \cdot m^{-2} \cdot K^{-1}}$ is achievable for VIG systems that have the potential to be mechanically stable. All results relate to VIG with 4 mm thick glass panes.

2 Experiments

2.1 General

The parameter of interest is the contribution of the spacer array to the total thermal heat transfer through VIG; it is quantified by the thermal conductance Λ_{spac}. For this purpose, the samples were prepared without an airtight seal. The measurements were conducted in an evacuable guarded hot-plate apparatus, whose vacuum chamber was evacuated to a pressure of 10^{-3} Pa in order to suppress heat conduction by gas in the space between the 4 mm thick glass panes. To ensure realistic system conditions, an external pressure load of 0.1 MPa was also applied.

2.2 Design and Measuring Principle of the Guarded Hot-Plate Apparatus

The evacuable guarded hot-plate apparatus is shown in Fig. 2. A circular metal plate (2) located in a vacuum chamber (1) acts as the hot plate. Its temperature is controlled by electrical heating. This plate is enclosed by two identical samples (5) on either side, which again are in contact with “cold” plates (3, 4). All plates are kept at constant

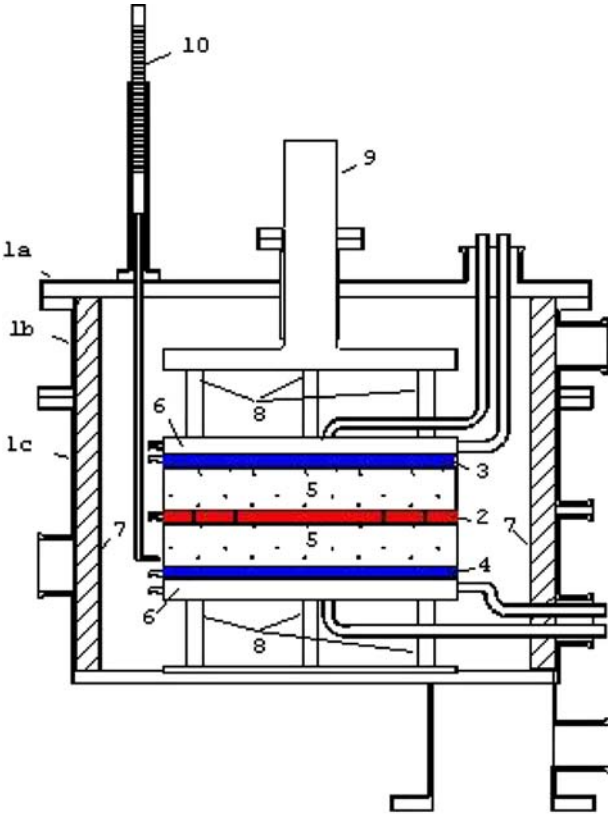

Fig. 2 Diagram of the evacuable guarded hot-plate apparatus: (1) vacuum chamber, (2) hot plate with two guard rings, (3) and (4) cold plates, (5) samples, (6) heat sinks, (7) insulation, (8) ceramic supports, (9) vacuum-tight guided stamp, and (10) three thickness sensors

temperatures with a temperature difference ΔT between the middle hot plate and the two outer cold plates. Heat flows from the hot plate through the samples to the cold plates. In order to establish a one-dimensional heat flux, the hot plate is surrounded by two concentrical guard rings, kept at the same temperature as the central plate. At steady-state conditions, the thermal conductance Λ of the sample in the vertical direction can be calculated by the electrical power P_{el} fed into the central hot plate:

$$\Lambda = \frac{P_{\mathrm{el}}}{2A_{\mathrm{MA}}\Delta T}. \tag{3}$$

A_{MA} is the area of the central hot plate (measuring area) and amounts to 152 cm^2. Each data point was measured for two different ΔT-values (10 K and 20 K). By extrapolating the result to $1/\Delta T = 0$, a remaining radial heat flow can be eliminated [6]. The value that results from this procedure is called Λ_{corr} in the following.

The vacuum chamber can be evacuated to gas pressures of 10^{-3} Pa. On the other hand, external pressure loads up to 4×10^5 Pa can be applied to the sample by a press (9).

2.3 Sample Preparation

Since samples of vacuum insulation glass are stiff and inhomogeneous, a very careful sample preparation is essential to reduce the uncertainties that otherwise occur when measuring them in the guarded hot-plate apparatus. First of all, experiments with a single glass pane showed imperfect thermal coupling to the plates of the apparatus. This could be improved by interconnecting the sample and the plates with flexible graphite foil with a thermal conductivity of $1\,\mathrm{W\cdot m^{-1}\cdot K^{-1}}$ to $5\,\mathrm{W\cdot m^{-1}\cdot K^{-1}}$ in the vertical direction (Fig. 3). Two foils of different thicknesses were tested, again with single glass panes as samples. Comparing the two foils, the 4 mm graphite foil is much softer than the 0.4 mm one and evens out irregularities in the thickness of the plates of the apparatus very well. Therefore, the 4 mm thick graphite foil yields the highest amount of coupling from the three possibilities tested; it is about six times better than without any foil (see Fig. 4).

The residual heat transfer resistance R_t between the glass panes and the plates of the apparatus, when connected by 4 mm thick graphite, is depicted as a function of the external pressure load p_ext in Fig. 5. R_t represents the series combination of the heat transfer resistances at both sample sides. In general, R_t is on the order of $10^{-2}\,\mathrm{m^2\cdot K\cdot W^{-1}}$, whereas the resistance of the VIG-samples, R_VIG, is expected to be about $1/(0.5\,\mathrm{W\cdot m^{-2}\cdot K^{-1}}) = 2\,\mathrm{m^2\cdot K\cdot W^{-1}}$, which is roughly a factor of 100 higher. Therefore, coupling due to the 4 mm thick graphite foil is sufficiently high and this foil was used for all following measurements. Although R_t is almost negligible in comparison to R_VIG, each measured thermal conductance of the VIG-samples was corrected by the respective value of R_t in order to guarantee accurate results:

$$\Lambda_\mathrm{VIG} = \left(\frac{1}{\Lambda_\mathrm{corr}} - R_\mathrm{t}\right)^{-1}. \tag{4}$$

However, a drawback of the graphite foil is the increase in radial heat flux, depicted in Fig. 4 by the error bars. In VIG parasitic heat flow becomes even more critical, because the thermal resistance through the sample (dominated by the evacuated space) is much higher than the lateral resistance (determined by the thermal conductivity of the graphite). That means a large amount of heat will flow laterally within the graphite instead of through the sample. To minimize this effect, the samples with graphite foil

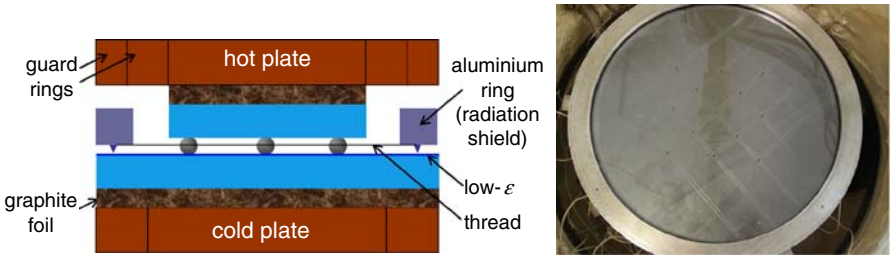

Fig. 3 Sample preparation with graphite foil for thermal coupling between glass panes and measuring plates, as well as grid of thread for positioning the spacers; *left*: schematic sketch of a vertical cut through the sample; *right*: view from above

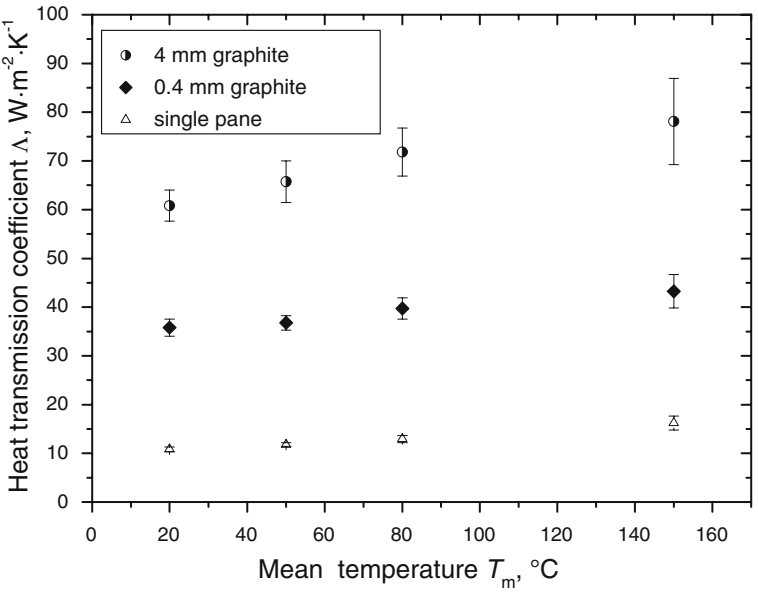

Fig. 4 Thermal conductance values of a single glass pane and panes coupled to the plates of the evacuated hot-plate apparatus with 0.4 mm and 4 mm thick graphite foil for an external pressure load of 0.1 MPa. All glass panes were 4 mm thick. The error bars represent the dimension of lateral heat flux

were chosen to be only as large as the central measuring area (Fig. 3), in order to force the heat to go through the sample. That was done for the two test series in Fig. 4 taken with graphite foil. These data in Fig. 4 show that this measure kept the relative amount of the radial heat flux (the radial heat flux divided by the total measured heat flux) at a constant level, when improving the thermal coupling with different types of graphite foil. That means, considering the data belonging to the same mean temperature, the radial heat flux changes proportionally to the heat flux through the sample. The relative amount of lateral heat flux is not higher than 10% at room temperature. Consequently, for VIG-samples with $\Lambda \approx 0.5\,\mathrm{W} \cdot \mathrm{m}^{-2} \cdot \mathrm{K}^{-1}$ an acceptably low lateral heat flux of about $0.05\,\mathrm{W} \cdot \mathrm{m}^{-2} \cdot \mathrm{K}^{-1}$ is expected. Subsequent measurements with VIG showed that it was even lower in many cases. Due to this fact, the use of the 4 mm thick graphite foil is still justified.

For the small samples just covering the central measuring area, the only radial way for heat to leave the central hot plate is by radiation. This radiative exchange between the sample and the insulation material of the surrounding walls is difficult to quantify, since the temperature of the insulation is not controlled during the measurements and thus may vary. Therefore, the radial radiative heat flux is the main source of the measurement uncertainty (see Sect. 2.4).

2.4 Radiation Effects

Beside the influence of the spacers, Λ_{VIG} of the above described VIG-samples includes radiation heat transfer, which was essentially reduced by using one low-ϵ coated glass

pane. The remaining amount of thermal radiation between the glass sheets, Λ_{rad}, had to be determined separately in order to extract the effect of the spacers from the overall thermal conductance Λ_{VIG}:

$$\Lambda_{\mathrm{spac}} = (\Lambda_{\mathrm{VIG}} - \Lambda_{\mathrm{rad}}) \frac{A_{\mathrm{MA}}}{A_{\mathrm{spac}}}, \tag{5}$$

where A_{MA} is the measuring area and A_{spac} is the actual area which is covered by the spacers (number of spacers multiplied by the second power of the spacer distance). The correction term $A_{\mathrm{MA}}/A_{\mathrm{spac}}$ needs to be included, because the area A_{spac} of the quadratic spacer array was never equal to the area of the circular central hot plate. Λ_{rad} was approximated by the formula for radiation exchange between infinitely expanded, parallel, and planar plates with a small temperature difference between the two plates:

$$\Lambda_{\mathrm{rad}} \approx 4\sigma T_{\mathrm{m}}^3 (\varepsilon_{\mathrm{low-e}}^{-1} + \varepsilon_{\mathrm{glass}}^{-1} - 1)^{-1}, \tag{6}$$

where σ is the Stefan-Boltzmann constant, T_{m} is the mean temperature between the two glass panes, and $\epsilon_{\mathrm{low-e}}$ and $\epsilon_{\mathrm{glass}}$ are the respective emissivities belonging to the surfaces of the sheets facing each other. For $\epsilon_{\mathrm{glass}}$ the literature value of 0.84 was taken. The error resulting from this approximation formula was estimated to be negligible for the temperature differences (10 K and 20 K) applied to the hot-plate apparatus within this work. Due to the symmetry of the VIG samples, the mean temperature T_{m} between the two glass panes is quite the same as the mean temperature T'_{m} between the hot and cold plates. The highest shift of T_{m} versus T'_{m} that is possible, because of different amounts of coupling to the hot and cold plates, is estimated in the following. According to Fig. 5, $R_{\mathrm{t}} < 0.04\,\mathrm{m}^2 \cdot \mathrm{K} \cdot \mathrm{W}^{-1}$ is valid for all measurements. If this heat transfer resistance belonged to one glass pane only and the other one was coupled perfectly to the plates of the apparatus, the temperature shift would be 0.4 K. Such an inaccuracy would cause a negligible error in Λ_{rad} compared to the uncertainty of $\varepsilon_{\mathrm{low-e}}$. That is why the temperatures of the hot and cold plates are sufficient to determine the mean radiation temperature and the temperatures of the glass panes did not have to be determined separately.

The emissivity of the low-ϵ coating, $\epsilon_{\mathrm{low-e}}$, was also measured in the guarded hot-plate apparatus, by "hanging" the low-ϵ coated glass pane between the plates of the apparatus. The experimental setup can be seen in Fig. 6. $\varepsilon_{\mathrm{low-e}}$ was calculated by solving the following set of equations:

$$q = \frac{\sigma\left(T_1^4 - T_2^4\right)}{\varepsilon_{\mathrm{app}}^{-1} + \varepsilon_{\mathrm{low-e}}^{-1} - 1}; \quad q = \frac{\sigma\left(T_2^4 - T_3^4\right)}{\varepsilon_{\mathrm{app}}^{-1} + \varepsilon_{\mathrm{glass}}^{-1} - 1} \tag{7}$$

q is the heat flux measured. The positions of the temperatures T_{i} are illustrated in Fig. 6. The temperature was assumed to be the same everywhere in the glass pane. The emissivity of the plates of the apparatus, $\varepsilon_{\mathrm{app}}$, was determined to be 0.9 by basically the same experimental setup, but without the suspended glass pane between the hot and cold plates. Finally, $\epsilon_{\mathrm{low-e}}$ amounts to 0.065 ± 0.005, which yields a radiative thermal conductance Λ_{rad} of $(0.37 \pm 0.03)\ \mathrm{W} \cdot \mathrm{m}^{-2} \cdot \mathrm{K}^{-1}$at room temperature. The

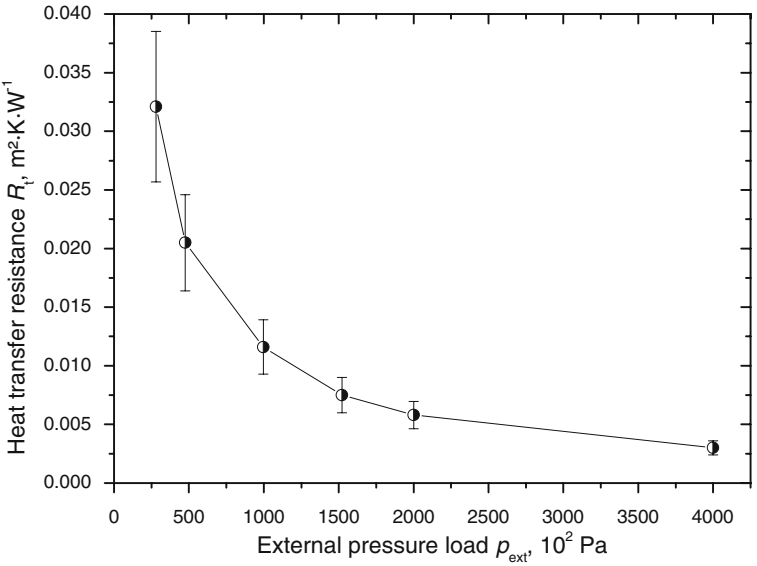

Fig. 5 Heat transfer resistance R_t between the plates of the apparatus and glass panes depending on the external pressure load at room temperature, for thermal coupling with 4 mm thick graphite foil and $p_{gas} = 10^{-3}$ Pa

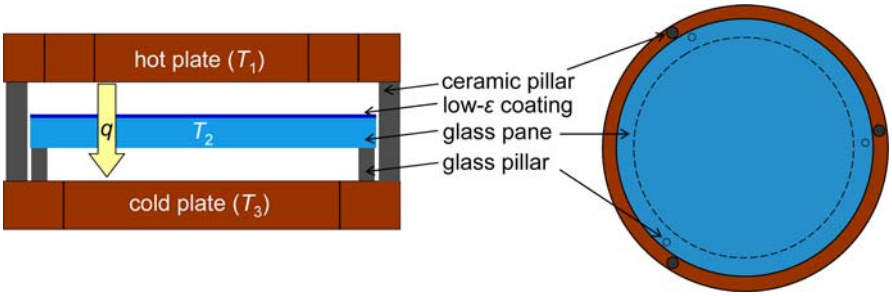

Fig. 6 Experimental setup for determining the emissivity of the low-ε coating in the guarded hot-plate apparatus, *left*: side view, *right*: top view. q is the heat flux through the glass pane

uncertainties include manufacturing fluctuations of the soft coatings and a degradation of the quality with time, since ε_{low-e} could not be re-evaluated for each measurement of Λ_{spac} for time reasons.

Additionally, $\varepsilon_{low-e} = 0.08 \pm 0.03$ was measured by an infrared spectrometer. The results of both measuring principles agree within the error limits. For processing the data belonging to the VIG-samples, the value that was detected in the guarded hot-plate apparatus was used, because of the identical measurement techniques.

Furthermore, radial radiative heat loss has to be considered. Since samples with spherical spacers are very unstable, it was necessary to keep them in the right position by means of a grid of thread, which was mounted to a ring of aluminum (Fig. 3). Comparison measurements with and without grid showed that the thermal

conductance of the VIG-samples was generally higher when measuring without grid. This can be explained by a not negligible radiation loss at the edge of the small glass panes, when the grid with the highly reflecting aluminum ring is absent. So the ring acts as a radiation shield, since it covers a large area on the side of the sample. This is also proved by the fact that the lateral heat flux decreases for measurements with the grid. It was estimated that the results for Λ_{spac} received without aluminum ring have to be corrected to lower values by about $0.04\,\mathrm{W}\cdot\mathrm{m}^{-2}\cdot\mathrm{K}^{-1}$ at room temperature.

3 Finite-Difference Model

In addition to the measurements in the guarded hot-plate apparatus, the heat transfer through the spacers was simulated by the PC-program HEAT3, which calculates the heat flux and temperature field in a given system by the finite-difference method. A cylindrical spacer was approximated by a cuboid with the same footprint, and spherical ones were built up by several cuboids. The thermal conductivities of glass and stainless steel were assumed to be $1\,\mathrm{W}\cdot\mathrm{m}^{-1}\cdot\mathrm{K}^{-1}$ and $10\,\mathrm{W}\cdot\mathrm{m}^{-1}\cdot\mathrm{K}^{-1}$, respectively. The low-$\varepsilon$ coating can be accounted for by an effective thermal conductivity in the space between the glass panes. A thermal contact resistance between the spacers and the glass panes can be included in terms of a direct program input.

4 Discussion

Figure 7 shows that the experimental thermal conductance Λ_{spac} increases almost linearly with decreasing spacer distance δ. From theory, however, a quadratic dependence is expected [8], if the thermal regions of the spacers do not overlap:

$$\Lambda_{\mathrm{spac}} = \Lambda'_{\mathrm{spac}}\frac{1}{\delta^2}, \tag{8}$$

whereas Λ'_{spac} is the thermal conductance of one single spacer in $\mathrm{W}\cdot\mathrm{K}^{-1}$.

This means, the smaller is δ the larger is the deviation between measurement and simulation; the difference reaches about 50 % for $\delta = 2\,\mathrm{cm}$. This was the case for both cylindrical spacers made from stainless steel and glass. The discrepancy could be explained by the fact that the theoretical values were calculated by assuming perfect thermal coupling of the cylinders and the glass panes, i.e., a thermal contact resistance of zero. In reality, the coupling is imperfect because of the surface roughness of the used materials (see Figs. 8, 9). However, it improves with an increasing spacer distance, because the load F on one spacer caused by the air pressure increases, since

$$p_{\mathrm{ext}} \equiv \mathrm{atm.} = \frac{F}{A} = \frac{F}{\delta^2}. \tag{9}$$

So the thermal contact resistance is only close to zero for large spacer separations, in our case for distances of about 4 cm. In the following, the quantity R_{c} is defined

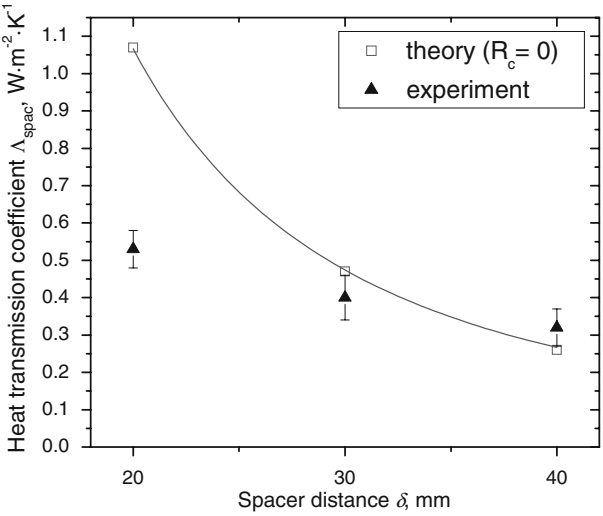

Fig. 7 Measured and calculated (*HEAT3*) thermal conductance values Λ_{spac} for cylindrical spacers of glass (diameter: 1 mm, height: 1 mm) at room temperature as a function of the spacer distance δ. The external pressure load was 0.1 MPa. The measurements were performed without grid, i.e., without radiation shield

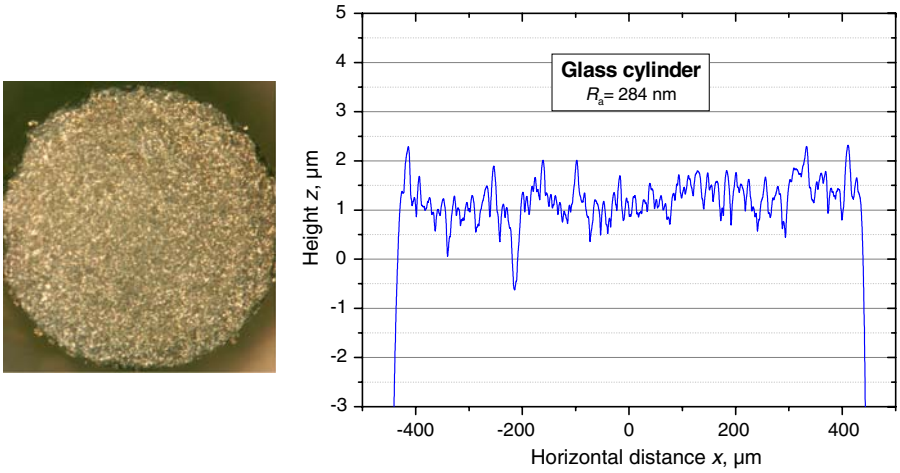

Fig. 8 Commercially available glass cylinder (diameter: 1 mm, height: 1 mm); *left*: microscope picture of top view, *right*: height profile of the end face. R_a denotes the average surface roughness of this surface. The profiles of different glass cylinders are quite similar

as the thermal contact resistance associated with heat flow through the unit area of a spacer; the units are $m^2 \cdot K \cdot W^{-1}$.

Heat transmission measurements with different external pressure loads p_{ext} were performed for cylinders of glass and stainless steel to prove this effect (see Fig. 10). Both depicted curves start with a steep slope, become flat, and finally reach a saturation value. For the spacers made from stainless steel, this value will coincide with the

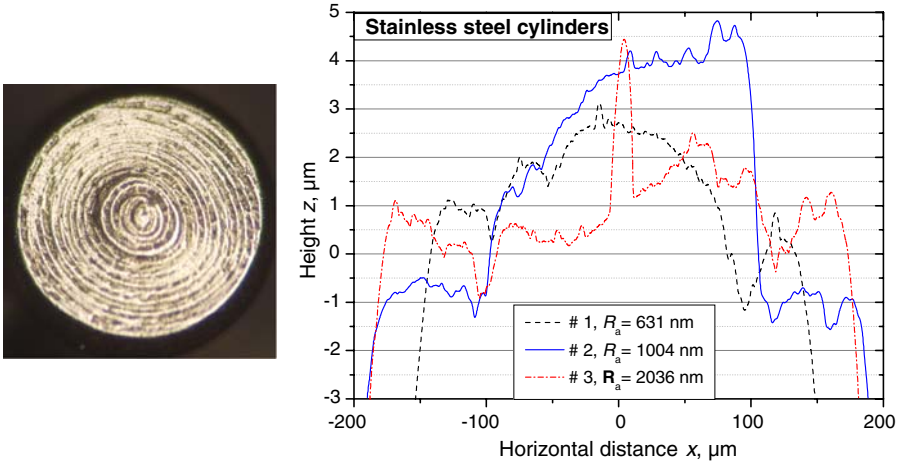

Fig. 9 Commercially available stainless steel cylinder (diameter: 0.5 mm, height: 1 mm); *left*: microscope picture of the top view, *right*: height profiles of the end faces belonging to three different stainless steel cylinders. R_a denotes the average surface roughness of these surfaces

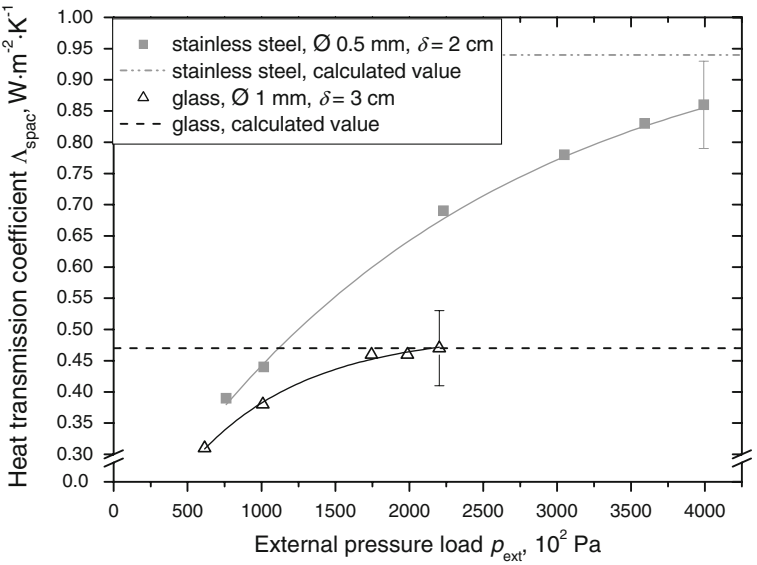

Fig. 10 Measured thermal conductances Λ_{spac} for cylindrical spacers made of glass (without grid, i.e., without radiation shield) and stainless steel (with grid, i.e., with radiation shield) as a function of external pressure load. The dotted lines show the theoretical values of Λ_{spac} for a thermal contact resistance of $0\,m^2 \cdot K \cdot W^{-1}$, calculated by means of HEAT3. δ is the spacer distance

calculated value for $R_c = 0\,m^2 \cdot K \cdot W^{-1}$ (HEAT3, dotted line) at external pressure loads of more than 4×10^5 Pa. The measurements with glass cylinders reach the calculated saturation value at an external pressure load of about 2×10^5 Pa. However, since these measurements were performed without a radiation shield, the thermal

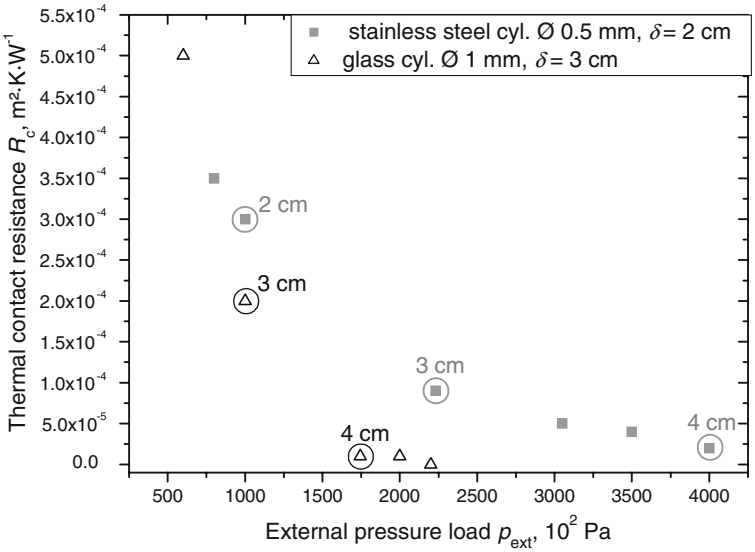

Fig. 11 Thermal contact resistance R_c between cylindrical spacers and glass panes as a function of the external pressure load p_{ext}. The corresponding spacer distances in VIG ($p_{ext} = 0.1$ MPa) are also marked. The given values for R_c were determined from the results of Fig. 10 by means of simulations

conductances obtained should be corrected to lower values, thus approaching the calculated value at higher external pressure loads.

At this point, it has to be remarked that all experimental data in Fig. 10 were corrected by the pressure–load-dependent heat transfer resistance R_t of Fig. 5. Consequently, the observed effect is caused by a changing contact resistance R_c between the spacers and the glass panes only. This is confirmed by Fig. 7, where the external pressure load and therefore, the heat transfer resistance R_t between the glass panes and the plates of the apparatus remain unchanged; only the load per spacer varies due to different spacer distances.

According to the system conditions of the measurements shown in Fig. 10, finite-difference simulations were performed with varying thermal contact resistance R_c. By comparing the theoretical thermal conductance values with the experimental ones of Fig. 10, a particular value for R_c could be related to each p_{ext} (see Fig. 11). Since the data for the glass cylinders were measured without grid, i.e., without radiation shield, the calculations may yield too low values for R_c (triangles in Fig. 11). This renders a direct quantitative comparison of the two curves more difficult. Nevertheless, it may be assumed that the steeper decrease for the glass cylinders is caused by the different loads for the single spacer and the different mechanical material properties of glass and stainless steel.

In addition, the different external pressure loads relate to certain spacer distances in VIG with a constant p_{ext} of 0.1 MPa, regarding the force F per spacer:

$$p_{ext}\delta_1^2 = \text{atm.} \cdot \delta_2^2. \tag{10}$$

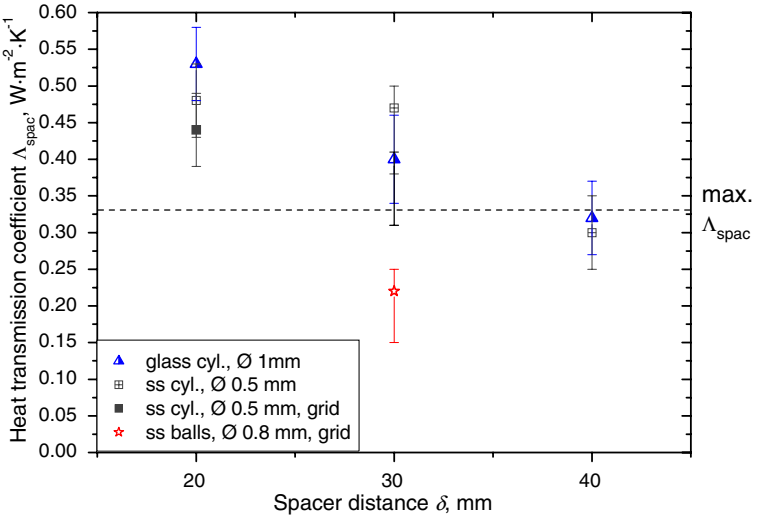

Fig. 12 Measured thermal conductances Λ_{spac} for different spacer systems at room temperature and an external load of 0.10 MPa; except for the stainless steel (ss) cylinders with $\delta = 3$ cm and the spheres $p_{ext} = 0.12$ MPa. The *dashed line* marks the maximum allowable Λ_{spac} that ensures the desired total heat transfer via VIG of $U_g < 0.5\,W \cdot m^{-2} \cdot K^{-1}$, assuming one low-$\varepsilon$ coating with $\varepsilon < 0.03$

For example, the force F per spacer in a VIG with realistic system conditions ($p_{ext} = 0.1$ MPa) and $\delta_2 = 4$ cm is equivalent to F of a system with $\delta_1 = 2$ cm and an external load of 0.4 MPa. Therefore, Fig. 11 can be interpreted as follows: the thermal contact resistance in VIG decreases from about $5 \times 10^{-4} m^2 \cdot K \cdot W^{-1}$ for very small spacer distances to nearly zero for $\delta = 4$ cm in both cases.

The thermal conductances Λ_{spac} measured for spherical and cylindrical spacer systems at room temperature are shown in Fig. 12. Generally, spheres cause less heat transfer because of their smaller contact area with the glass panes. The best result received was $0.22\,W \cdot m^{-2} \cdot K^{-1}$ for stainless steel balls with a diameter of 0.8 mm at spacer distances of 3 cm. Load tests, however, showed a strongly reduced mechanical stability of evacuated glazing containing spherical spacers [9]. The small contact areas may lead to cracks in the glass panes, even at low mechanical loads. That is why cylindrical spacers are preferred for the VIG design, in spite of their worse thermal performance.

In Fig. 12, it can also be seen that the cylinders made from stainless steel with a diameter of 0.5 mm lead to slightly smaller conductances than the thicker glass cylinders of 1 mm in diameter, although the thermal conductivity of stainless steel is about 10 times higher than the thermal conductivity of glass. At spacer separations of 4 cm, $\Lambda_{spac} < 0.33\,W \cdot m^{-2} \cdot K^{-1}$ is valid for both cylinder types. This range is thermally acceptable in the above described VIG system (see Fig. 1). However, according to Collins et al. a spacer separation of 4 cm leads to high external tensile stress above the spacers in a 4 mm thick glass pane [10]. On the other hand, thicker glass could be used to reduce these stresses. It is also possible to use an already stable cylinder matrix with a smaller spacer distance together with two highly efficient low-ϵ

Table 1 Comparison of experimental thermal conductance values due to the spacers; this work: stainless steel cylinders, diameter = 0.5 mm, height = 1 mm; Wilson et al.: stainless steel cylinders, diameter ≈ 0.54 mm, height = 0.1 mm to 0.2 mm [11].

Spacer separation	Λ_{spac} (this work)	Λ_{spac} (Wilson et al. [11])
20 mm	$(0.44 \pm 0.05)\ \mathrm{W \cdot m^{-2} \cdot K^{-1}}$	$1.38\ \mathrm{W \cdot m^{-2} \cdot K^{-1}}$
40 mm	$(0.30 \pm 0.05)\ \mathrm{W \cdot m^{-2} \cdot K^{-1}}$	$0.34\ \mathrm{W \cdot m^{-2} \cdot K^{-1}}$

coatings, in order to receive an overall acceptable VIG design. According to Collins, the suggested changes yield stable evacuated windows in general, but concerning the particular spacers used in the framework of this paper, the stability has to be tested first. Indeed, to ensure good mechanical properties of the glazing, stainless steel cylinders are more appropriate than glass cylinders.

Finally, the measurement results of the stainless steel cylinders were compared to the data of the research group at the University of Sydney [11] (see Table 1). For a spacer separation of 40 mm, the heat transmission through the spacers measured within the scope of this paper is a little lower (regarding the correction to a lower value because of measuring without radiation shield) than the value of the Australian group. This results from a slightly smaller spacer diameter and up to 10 times higher cylinders in the case presented here. The data for a spacer separation of 20 mm show a much higher deviation, since the thermal contact resistance R_c, which depends on the load per pillar and therefore on the spacer separation, is much more critical for the spacers used in this paper than for the pillars of the other research group.

5 Conclusion

Experimental investigations show that the thermal contact resistance between a spacer and glass pane in vacuum glazing may significantly influence the heat transfer. The experimental determination of the heat transfer via the spacers was performed with an evacuable guarded hot-plate apparatus. In this context, a modified sample preparation method was applied to achieve a sufficiently high thermal coupling between the glass panes and the measuring plates of the guarded hot-plate apparatus. It could be shown that adding a radial radiation shield at the fringe of the sample reduces systematic errors due to radial heat losses.

Accounting for the mechanical properties of the VIG design, cylindrical spacers, especially when made from stainless steel, are preferable. For the stainless steel cylinders investigated, spacer arrays with $\Lambda_{spac} \leq 0.44\,\mathrm{W \cdot m^{-2} \cdot K^{-1}}$ were found by experiments. Those spacer systems may be both mechanically and thermally acceptable, if the original VIG design is modified in an appropriate way, like using two low-ϵ coatings with $\varepsilon < 0.03$ or thicker glass panes. Thus, the measurements proved that a stable evacuated window with a U_g-value of about $0.5\ \mathrm{W \cdot m^{-2} \cdot K^{-1}}$ is feasible. However, future load tests are required to guarantee the stability of VIG with certain cylinders. Furthermore, a knowledge of the thermal contact resistance between the

used cylinders and the glass panes is highly relevant for further simulations and the optimization of evacuated glazing.

Acknowledgments The scientific investigations have been carried out within the research project "Vacuum Insulation Glass—VIG", which was supported by the German Federal Ministry of Economics and Technology (2004–2006, FkZ 0327366). During this project, the feasibility of Vacuum Insulation Glass has been shown. A current research project, also funded by the German Federal Ministry of Economics and Technology (FkZ 0327419), is focusing on developing a manufacturing process for serial production of VIG. This is to be completed by the end of 2011 (more information: www.vig-info.de).

References

1. R.E. Collins, A.C. Fischer-Cripps, J.Z. Tang, Sol. Energ. **49**, 333 (1992)
2. H. Weinläder, H.-P. Ebert, J. Fricke, VIG—Vacuum Insulation Glass, in *Proceedings of 7th International Vacuum Insulation Symposium*, 2005, pp. 197–204
3. R.E. Collins, C.A. Davis, C.J. Dey, S.J. Robinson, J.-Z. Tang, G.M. Turner, Int. J. Heat Mass Transfer **36**, 2553 (1993)
4. T.M. Simko, A.H. Elmahdy, R.E. Collins, ASHRAE Trans. **105**(Part 2), 891 (1999)
5. R.E. Collins, L. Poladian, B.A. Pailthorpe, R.C. McPhedran, Aust. J. Phys. **44**, 73 (1991)
6. U. Heinemann, J. Hetfleisch, R. Caps, J. Kuhn, J. Fricke, Advances in Thermal Insulation, in *Proceedings of Eurotherm Seminar No. 44*, 1995, pp.155–164
7. R.E. Collins, A.C. Fischer-Cripps, Aust. J. Phys. **44**, 545 (1991)
8. R.E. Collins, S.J. Robinson, Sol. Energ. **47**, 27 (1991)
9. *Abschlussbericht zum Verbund Vakuum-Isolierglas (VIG)*, FkZ 0327366 (Verband Deutscher Maschinen- und Anlagenbau e.V. (VDMA), Frankfurt am Main, 2007), pp. 23–24
10. R.E. Collins, G.M. Turner, A.C. Fischer-Cripps, J.-Z. Tang, T.M. Simko, C.J. Dey, D.A. Clugston, Q.-C. Zhang, J.D. Garrison, Build. Environ. **30**, 459 (1995)
11. C.F. Wilson, T.M. Simko, R.E. Collins, Sol. Energ. **63**, 393 (1998)